Available online at www.sciencedirect.com
ScienceDirect
Trans. Nonferrous Met. Soc. China 33(2023) 518−530
Transactions of Nonferrous Metals Society of China
www.tnmsc.cn

Prediction of elastic properties of face-centered cubic high-entropy alloys by machine learning

Shen WANG, Da LI, Jun XIONG

Key Laboratory of Advanced Technologies of Materials, Ministry of Education,
College of Materials Science and Engineering, Southwest Jiaotong University, Chengdu 610031, China

Received 20 October 2021; accepted 24 February 2022

Abstract: The machine learning (ML) models were proposed for predicting elastic properties of face-centered-cubic (FCC) high-entropy alloys (HEAs). The data set was from the first-principles calculation, which contained 186 samples. The goodness-of-fit (R^2) values of predicted bulk modulus (B) and shear modulus (G) in the test set were 0.81 and 0.84, respectively. According to the results of ML, CoNiCuMoW HEAs have the largest B, G, elastic modulus (Y) and good ductility (G/B≤0.57) among the FCC HEAs with equal components. The first-principles calculation results show that the elastic anisotropy of $(CoNiCuMo)_{1-x}W_x$ HEAs increases and ductility decreases with increasing W content. According to the analysis of charge density difference, there is obvious charge accumulation at W—W and W—Mo bonds, indicating the directional covalent bonds formed between W atoms and their neighboring atoms.
Key words: elastic modulus; face-centered cubic high-entropy alloys; first-principles calculations; machine learning

1 Introduction

Face-centered cubic (FCC) high-entropy alloys (HEAs) have significant prospects in engineering applications because of their cryogenic fracture resistance [1] and radiation resistance [2−6] compared with traditional alloys. In addition, FCC HEAs have higher swelling resistance under radiation than body-centered cubic (BCC) HEAs [7], and they are expected to become the structural materials of nuclear reactors. At present, the design of FCC HEAs is mainly based on the transition elements at the fourth period in the periodic table, such as Cr, Mn, Fe, Co, Ni and Cu, and the properties of FCC HEAs still have great space for improvement in terms of composition design.

Elastic modulus is an important mechanical property for materials [8−10], representing the binding force between atoms. Higher elastic modulus means that the atoms in alloys bond more firmly, which is generally beneficial to their applications as structural materials. First-principles calculation is an effective method to investigate the elastic properties of HEAs. For example, ZHANG et al [11] have predicted the elastic properties of CrMnFeCoNi HEAs by first-principles calculation, and the predicted results are in good agreement with the experimental values. ZHAO et al [12] have investigated the effect of Al solute concentration on mechanical properties of $Al_xFeCuCrNi$ HEAs by first-principles study, and the results show that increasing Al concentration enhances the elastic modulus, bulk modulus and shear modulus. However, it reduces the ductility from the calculation results of Cauchy pressure.

Although first-principles calculation can predict the elastic properties of HEAs, it is still difficult to find the composition of HEAs with

Corresponding author: Da LI, Tel: +86-15928830352, E-mail: hardfacing@home.swjtu.edu.cn
DOI: 10.1016/S1003-6326(22)66124-7

excellent properties because of the diversity of element combinations. Machine learning (ML) has important applications in studying the properties and mechanism of materials [13,14], including HEAs. For example, ZHOU et al [15] have used artificial neural network (ANN), convolutional neural network (CNN) and support vector machine (SVM) to predict solid solution (SS), amorphous metallic (AM) and intermetallic (IM) phases in HEAs. BOY et al [16] have used gradient boosting regression model to predict elastic modulus of low entropy alloys, medium entropy alloys and HEAs.

The above researchers successfully proposed generalized models for predicting the properties of HEAs. However, the value of ML lies more in mining the components of alloys with desired properties, and there are few studies about the composition design of FCC HEAs through ML method. Compared with previous studies, this work proposed the models for predicting elastic properties of FCC HEAs by using ML method and first-principles calculation. The FCC HEAs with desired elastic properties were designed through the ML model, and their elastic properties were further investigated by first-principles and fitting equation of state (EOS).

2 Methods and calculation details

2.1 Calculation method of elastic properties

In the present study, we employed the Cambridge Sequential Total Energy Package [17] based on the density functional theory within the generalized gradient approximation, treated by Perdew−Burke−Ernzerhof exchange-correlation potentials to calculate elastic properties of HEAs. The ultrasoft pseudopotentials were used to represent the interactions between the ionic cores and the valence electrons. The plane wave cutoff energy was 450 eV according to the convergence test of single-point energy. The Brillouin zone sampling was performed using special k-points generated by the MONKHORST−PACK [18] scheme with density parameter of 0.03 Å^{-1}. A high convergence tolerance level (the maximum force is about 0.05 eV/Å, and the maximum stress is about 0.1 GPa) was also chosen. We established HEAs models by using the special quasi-random structure (SQS) method [19]. The "mcsqs" model [20] installed in Alloy Theoretical Automated Toolkit (ATAT) was used to generate SQS supercells.

The equivalent elastic constants of cubic crystal (c_{11}, c_{12}, c_{44}) can be calculated by first-principles method [21,22], and bulk modulus (B) and shear modulus (G) can be obtained by the approximation in Ref. [23]:

$$B=(c_{11}+2c_{12})/3 \tag{1}$$

$$G=[5c_{44}(c_{11}-c_{12})/(4c_{44}+3(c_{11}-c_{12}))+(c_{11}-c_{12}+3c_{44})/5]/2 \tag{2}$$

The elastic modulus (Y) and Poisson ratio (v) can be obtained by B and G:

$$Y=9BG/(3B+G) \tag{3}$$

$$v=(3B-2G)/(6B+2G) \tag{4}$$

The elastic properties of HEAs at high temperature can be obtained by the derivative of equation of Gibbs function $G(V, P, T)$:

$$B(P,T)=V\left(\frac{\partial^2 G(V,P,T)}{\partial V^2}\right)_{P,T} \tag{5}$$

where P, V and T represent pressure, volume and temperature, respectively, and $G(V, P, T)$ can be obtained by EOS:

$$G(V, P, T)=E_0(V)+PV+F_{vib}(V, T)+F_{el}(V, T) \tag{6}$$

where $E_0(V)$ is the total energy at ground state, $F_{vib}(V, T)$ is the free energy of lattice vibration, which can be obtained by quasi-harmonic Debye approximation [24,25], and $F_{el}(V, T)$ is the thermo-electric free energy, which can be calculated by Sommerfeld approximation [25].

2.2 Details of ML methods

The 186 samples were from the results of the first-principles calculation. 80% of total samples were used for training ML models and the rest 20% samples were used as the test set. Previous studies have shown that the solid solution phase of HEAs is easy to form when $\Omega\geq1.1$ and $\delta\leq6.6\%$ [26], where Ω is defined as a parameter of the entropy of mixing timing the average melting temperature of the elements over the enthalpy of mixing, and δ is the mean square deviation of the atomic size of elements. The FCC HEAs will be stable when valence electron concentration (VEC) is not less than 8.0 [27]. The random compositions of HEAs with five principal components generated as samples set all satisfy the above conditions about the formation of the FCC solid solution phase.

We selected the main group element (Al only), transition elements in the fourth period, including Ti, V, Cr, Mn, Fe, Co, Ni, and Cu and the refractory metal elements in the fifth and sixth periods, including Nb, Mo, Ta, and W, as the components of HEAs (the VECs of Nb, Mo, Ta and W are relatively large). The atomic radii of these elements are close to those of the transition elements in the fourth period, which will be helpful for the formation of the FCC solid solution. The frequency of each element appearing in the sample set is shown in Fig. 1. Each element occurs in high frequency, and the model trained with such samples has good adaptability in new data.

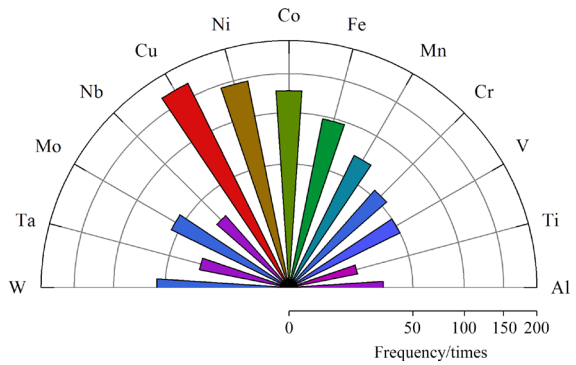

Fig. 1 Frequency of each element appearing in sample set

We extracted the component contents and the statistics of element properties as features for describing HEAs. The vectors including 13 values were established to describe the components of HEAs, whose examples are shown in Fig. 2. We also selected mixing entropy (ΔS_{mix}), mixing enthalpy (ΔH_{mix}), mean (μ) and standard deviation (σ) of element properties, including B, G, melting temperature, valence electron number, atomic radius, proton number, first ionization energy, density, cohesive energy, electronegativity, and second ionization energy. The calculations of μ and σ are as follows:

$$\mu=\sum_{i=1}^{n}c_i x_i \tag{7}$$

$$\sigma=\sqrt{\sum_{i=1}^{n}c_i\left(x_i-\mu\right)^2} \tag{8}$$

where c_i and x_i represent the property and mole fraction of the ith element in HEAs, respectively. The 37 selected features for describing HEAs are listed in Table 1.

The gradient boosting decision tree (GBDT) was used for predicting the elastic properties of HEAs because they are suitable for the nonlinear prediction and will not be affected by multi-collinearity between features.

3 Results and analysis

The goodness of fit (R^2), mean absolute percentage error (MAPE), mean absolute error (MAE), mean square error (MSE) and root mean square error (RMSE) of predicted B and G in the test set (37 samples in total) are listed in Table 2. The comparison between predicted elastic and shear moduli and their true values in the test set is shown in Fig. 3. The models performed well on the test set, indicating that generalized models were obtained in this work.

It can be seen from Table 3 that the predicted elastic properties of FCC CrMnFeCoNi HEA are close to those of other researchers, indicating the reliability of our model.

We also analyzed the relative importance of the adopted features. The ranking by the percentage of contribution to GBDT (top 10) is shown in Fig. 4. G_avg and r_avg are the most important features for predicting B and G.

In order to analyze the correlation between each feature and B or G in sample set, we calculated the Pearson correlation coefficient between them, as listed in Table 4. There is a high positive correlation between the mole fraction of W and B or G.

	Al	Ti	V	Cr	Mn	Fe	Co	Ni	Cu	Nb	Mo	Ta	W
CrMnFeCoNi:	[0	0	0	0.2	0.2	0.2	0.2	0.2	0	0	0	0	0]
$AlCrFeNi_2Cu$:	[0.17	0	0	0.17	0	0.17	0	0.33	0.17	0	0	0	0]
Cr MnFeCoNiNb:	[0	0	0	0.17	0.17	0.17	0.17	0.17	0	0.17	0	0	0]
CuMnFeCoNiCu:	[0	0	0	0.17	0.17	0.17	0.17	0.17	0.17	0	0	0	0]
⋮							⋮						

Fig. 2 Examples of feature vectors for describing components of HEAs

Table 1 Selected features for describing HEAs

Name	Label	Name	Label
Mole fraction of Al	Al_mf	μ of atomic radius	r_avg
Mole fraction of Ti	Ti_mf	μ of proton numbers	Z_avg
Mole fraction of V	V_mf	μ of first ionization energies	IE1_avg
Mole fraction of Cr	Cr_mf	μ of densities	S_avg
Mole fraction of Mn	Mn_mf	μ of cohesive energies	CE_avg
Mole fraction of Fe	Fe_mf	μ of electronegativities	EN_avg
Mole fraction of Co	Co_mf	μ of second ionization energies	IE2_avg
Mole fraction of Ni	Ni_mf	σ of bulk modulus	B_sd
Mole fraction of Cu	Cu_mf	σ of shear modulus	G_sd
Mole fraction of Nb	Nb_mf	σ of melting temperatures	Tm_sd
Mole fraction of Mo	Mo_mf	σ of valence electron numbers	VE_sd
Mole fraction of Ta	Ta_mf	σ of atomic radius	r_sd
Mole fraction of W	W_mf	σ of proton numbers	Z_sd
Entropy of mixing	deta_S	σ of first ionization energies	IE1_sd
Enthalpy of mixing	deta_H	σ of densities	DS_sd
μ of bulk modulus	B_avg	σ of cohesive energies	CE_sd
μ of shear modulus	G_avg	σ of electronegativities	EN_sd
μ of melting temperatures	Tm_avg	σ of second ionization energies	IE2_sd
μ of valence electron numbers	VE_avg		

Table 2 R^2, MAPE, MAE, MSE and RMSE of predicted B and G in test set

Parameter	R^2	MAPE/%	MAE/GPa	MSE/GPa^2	RMSE/GPa
GBDT-B	0.81	9.2	14.4	290.3	17.0
GBDT-G	0.84	7.9	6.9	72.3	8.5

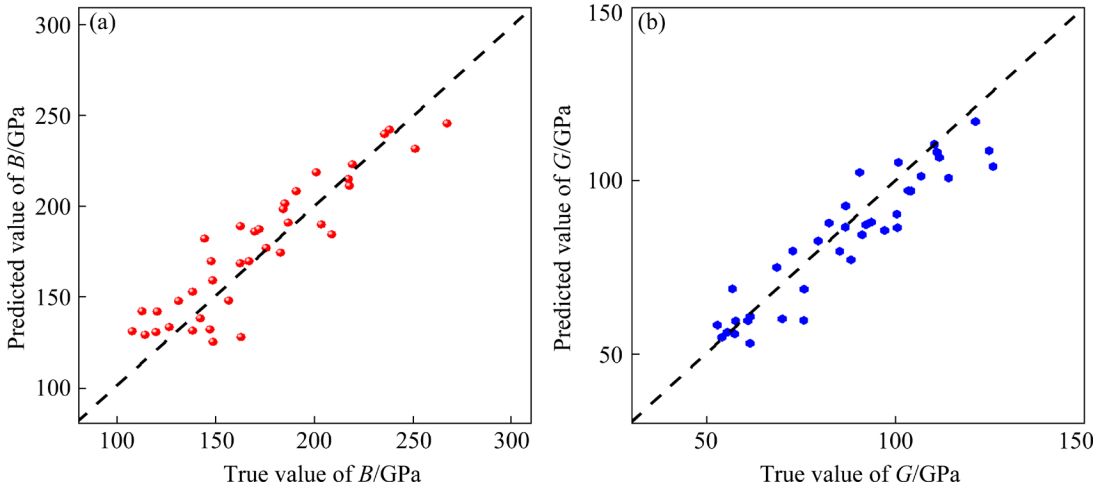

Fig. 3 Comparison of predicted bulk modulus (a) and shear modulus (b) with their true values in test set

We used the trained models to predict elastic modulus and G/B of HEAs with equal components which satisfy the criterion of the solid solution phase formation ($\Omega \geq 1.1$ and $\delta \leq 6.6\%$) and the stabilization of FCC phase (VEC≥8), as shown in Figs. 5−7. According to Pugh criterion [34], the

Table 3 Predicted elastic properties of FCC CrMnFeCoNi HEAs from ML in this work and values calculated by SQS, coherent potential approximation (CPA) and experimental values in other works

Source	*B*/GPa	*G*/GPa	*Y*/GPa	*v*	*G*/*B*
Predicted by ML (0 K)	183	99	252	0.260	0.540
EMTO-CPA (0 K) [28,29]	186	111	276	0.246	0.613
EMTO-CPA (0 K) [29]	176	106	266	0.246	0.602
EMTO-CPA (0 K) [30]	184	79	207	0.313	0.429
VASP-SQS (0 K) [30]	131	97	233	0.204	0.740
Expt. (300 K) [31]	144	80	202	0.265	0.555
Expt. (300 K) [32]	129	61	157	0.297	0.472
Expt. (300 K) [33]	143	80	202	0.265	0.559
Expt. (55 K) [33]	145	86	215	0.253	0.593

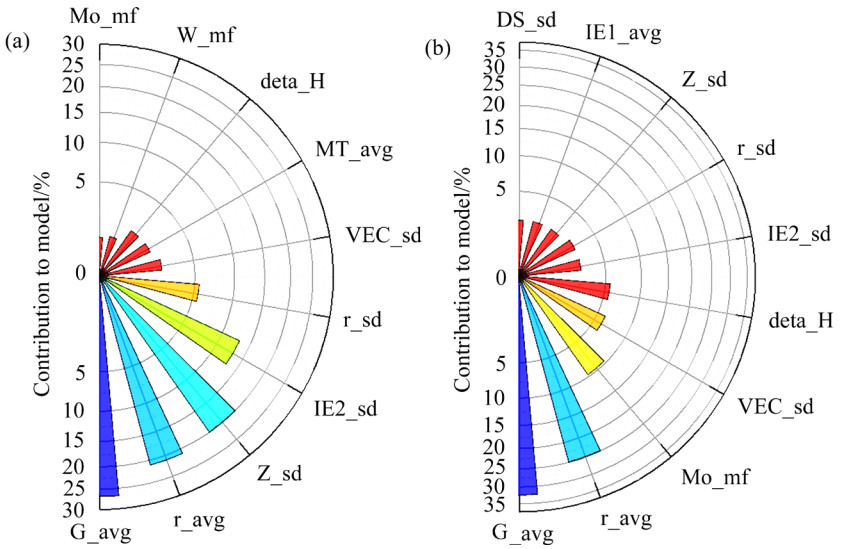

Fig. 4 Feature importance of GBDT model for bulk modulus (a) and shear modulus (b)

Table 4 Correlation coefficient between each feature and *B* or *G* in sample set

Feature	*B*	*G*	Feature	*B*	*G*
Al_mf	−0.264	−0.300	r_avg	−0.394	−0.363
Ti_mf	−0.191	−0.138	Z_avg	0.135	0.239
V_mf	−0.132	−0.239	IE1_avg	0.296	0.457
Cr_mf	0.262	0.111	DS_avg	0.248	0.358
Mn_mf	0.124	0.252	CE_avg	0.097	0.129
Fe_mf	0.155	0.119	EN_avg	0.024	0.010
Co_mf	0.167	0.183	IE2_avg	−0.203	−0.169
Ni_mf	−0.013	−0.042	B_sd	0.157	0.308
Cu_mf	−0.454	−0.418	G_sd	0.236	0.298
Nb_mf	−0.294	−0.330	MT_sd	0.029	0.143
Mo_mf	−0.046	−0.023	VEC_sd	−0.604	−0.663
Ta_mf	−0.334	−0.316	r_sd	−0.558	−0.491
W_mf	0.388	0.482	Z_sd	0.046	0.158
deta_S	−0.074	−0.109	IE1_sd	−0.226	−0.384
deta_H	0.312	0.374	DS_sd	0.118	0.217
B_avg	0.353	0.404	CE_sd	0.004	0.140
G_avg	0.629	0.672	EN_sd	−0.223	−0.188
MT_avg	0.263	0.296	IE2_sd	−0.546	−0.524
VEC_avg	−0.075	0.007			

value of *G*/*B* reflects the ductility or brittleness of materials. When *G*/*B*≤0.57, the materials have good ductility and when *G*/*B*>0.57, the materials are brittle. From Fig. 5, CoNiCuMoW HEA has the largest *B*, *G* and *Y* under the condition of *G*/*B*≤0.57.

In order to investigate the effect of component contents on the elastic modulus of HEAs, we also used the ML model to predict the *B*, *G* and *Y* of CoNiCuMoW HEAs with unequal components (569 in total), as shown in Figs. 8−10, and these HEAs also satisfy the criterion of solid solution phase formation and the stabilization of FCC phase. The colored percentage diagram below represents the content of each component in CoNiCuMoW HEAs. The *B*, *G* and *Y* increase greatly with increasing W content, and decrease slightly with increasing Cu content. Besides, only *B* has significant increase with increasing Mo content.

Since W is the critical element on the elastic modulus of CoNiCuMoW HEAs, it is meaningful to study the effect of W content on its elastic properties and mechanism further. Four supercells

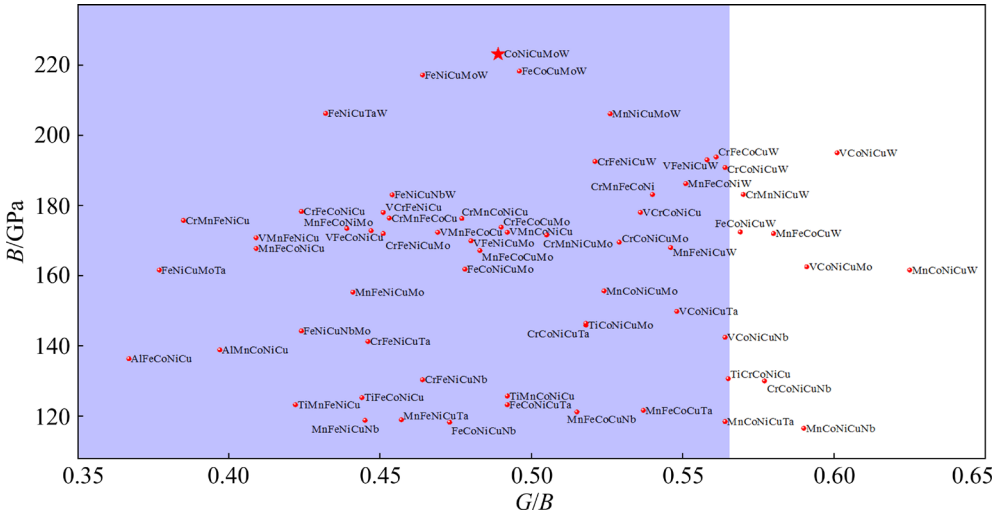

Fig. 5 Predicted bulk modulus (B) and G/B of FCC HEAs with equal components

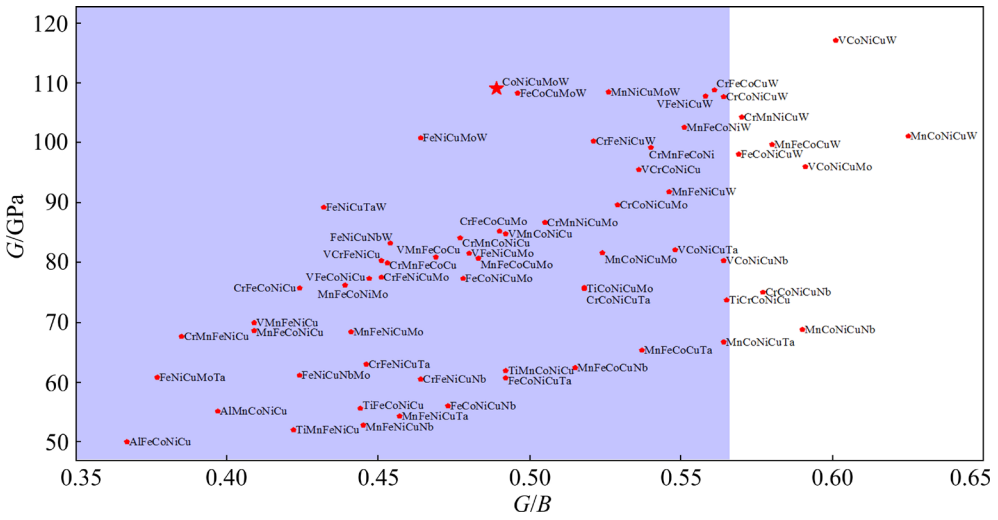

Fig. 6 Predicted shear modulus (G) and G/B of FCC HEAs with equal components

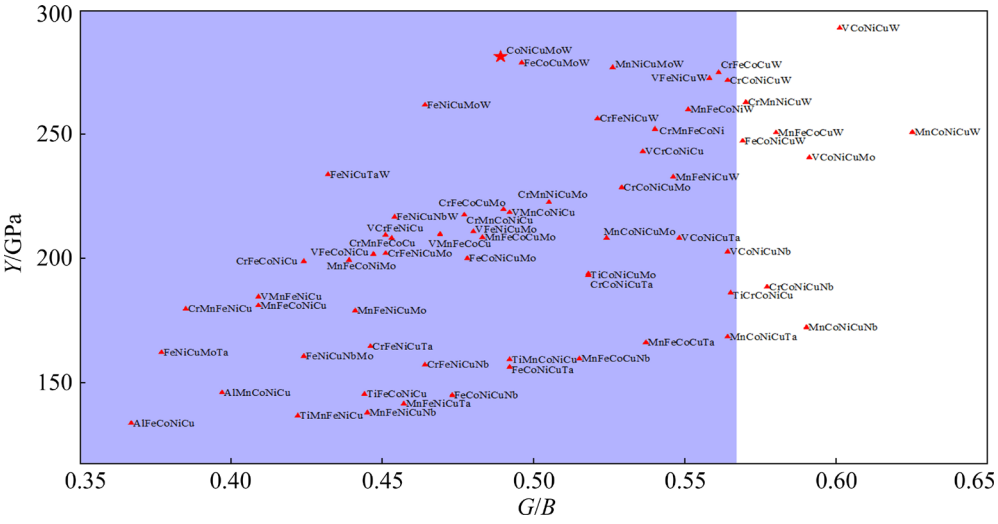

Fig. 7 Predicted elastic modulus (Y) and G/B of FCC HEAs with equal components

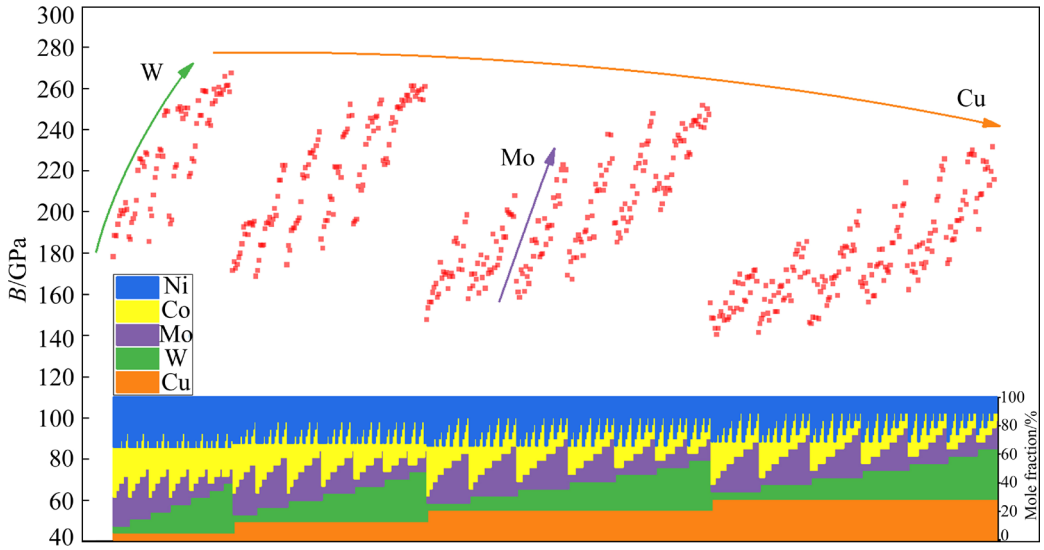

Fig. 8 Predicted bulk modulus (B) of CoNiCuMoW HEAs with unequal components

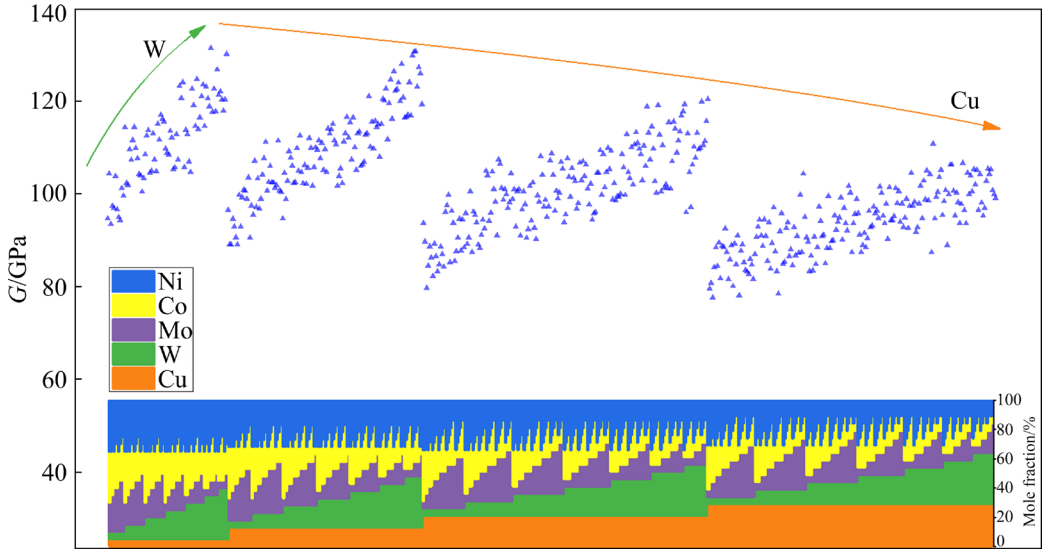

Fig. 9 Predicted shear modulus (G) of CoNiCuMoW HEAs with unequal components

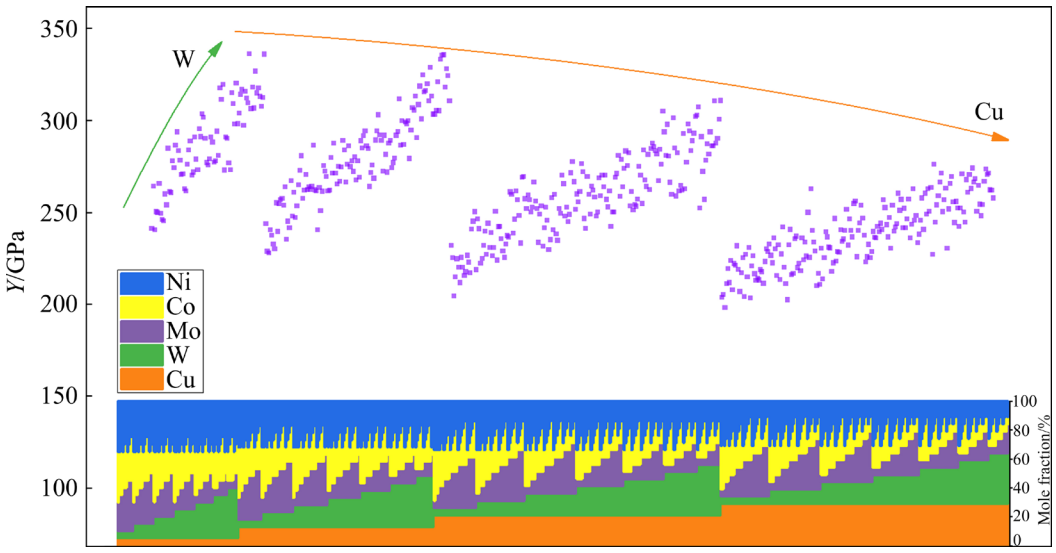

Fig. 10 Predicted elastic modulus (Y) of CoNiCuMoW HEAs with unequal components

with $2a\times2a\times2a$ lattice parameters (a is the lattice constant of the single FCC cell) were established, which are shown in Fig. 11. The chemical formulas are $Co_8Ni_8Cu_8Mo_8$, $Co_7Ni_7Cu_7Mo_7W_4$, $Co_6Ni_6Cu_6Mo_6W_8$ and $Co_5Ni_5Cu_5Mo_5W_{12}$, respectively. These HEAs can be written as a function of W content: $(CoNiCuMo)_{1-x}W_x$ (x=0, 0.125, 0.250 and 0.375). These HEAs also satisfy the criterion of the solid solution phase formation ($\Omega\geq1.1$ and $\delta\leq6.6\%$) and the stabilization of FCC phase (VEC≥8) except the VEC of $(CoNiCuMo)_{0.625}W_{0.375}$, as listed in Table 5.

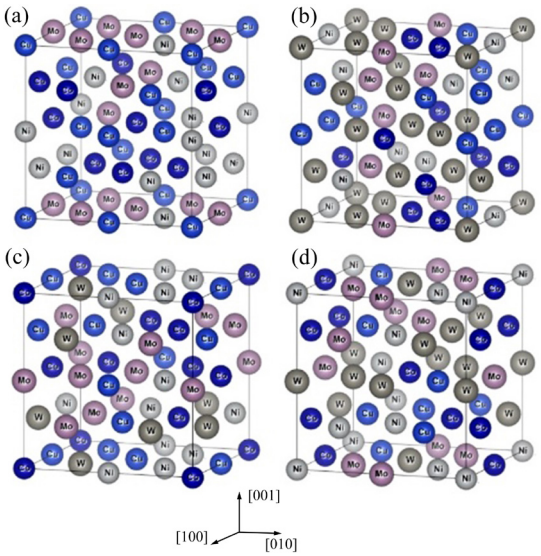

Fig. 11 Supercells of $(CoNiCuMo)_{1-x}W_x$ HEAs: (a) CoNiCuMo; (b) $(CoNiCuMo)_{0.875}W_{0.125}$; (c) $(CoNiCuMo)_{0.750}W_{0.250}$; (d) $(CoNiCuMo)_{0.625}W_{0.375}$

The mechanical properties of the FCC $(CoNiCuMo)_{1-x}W_x$ HEAs are shown in Fig. 12. The value of $c_{12}-c_{44}$ represents Cauchy pressure. If $c_{12}-c_{44}>0$, the material usually has good ductility,

Table 5 Parameters of $(CoNiCuMo)_{1-x}W_x$ HEAs related to phase formation

HEA	Ω	δ/%	VEC
CoNiCuMo	5.2	4.8	9.0
$(CoNiCuMo)_{0.875}W_{0.125}$	5.5	5.3	8.6
$(CoNiCuMo)_{0.750}W_{0.250}$	5.5	5.5	8.3
$(CoNiCuMo)_{0.625}W_{0.375}$	5.6	5.5	7.9

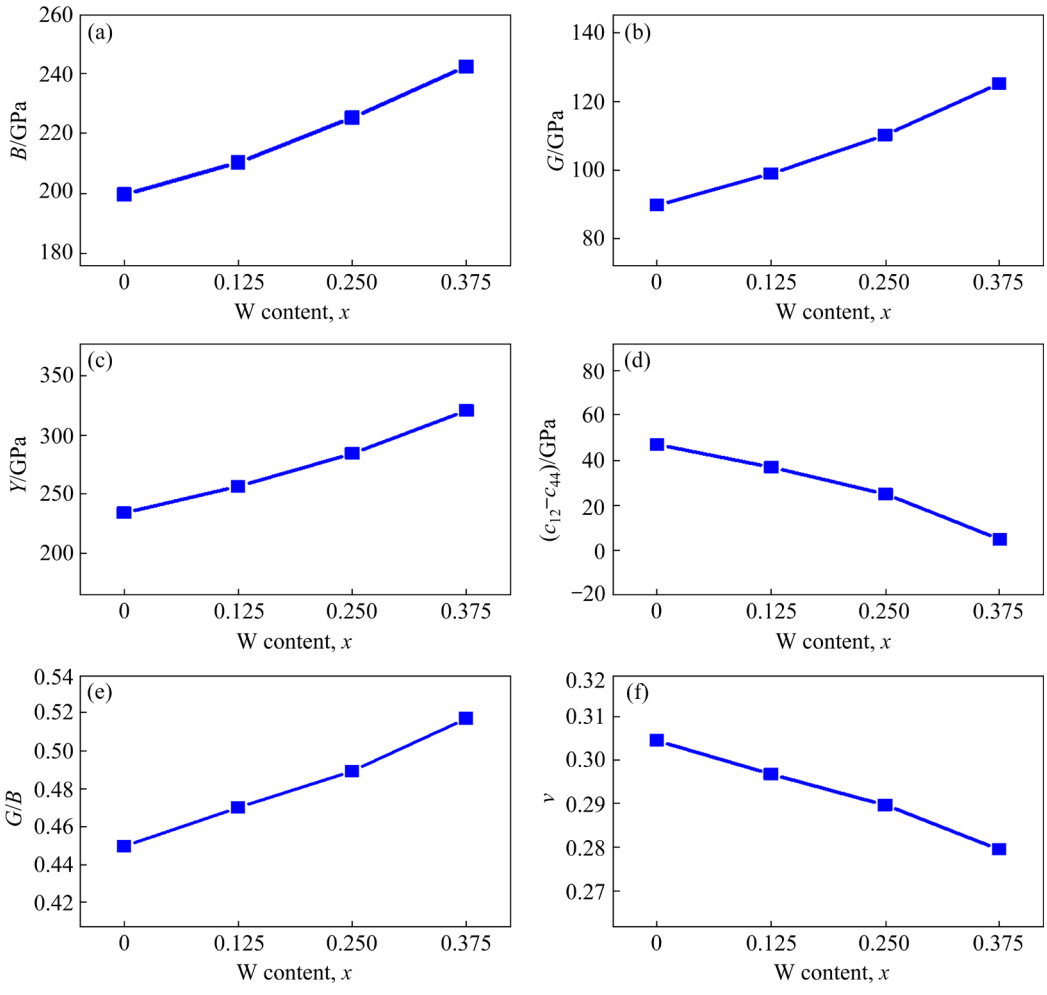

Fig. 12 Mechanical properties of FCC $(CoNiCuMo)_{1-x}W_x$ HEAs from first-principles calculation

and the larger the value is, the better the ductility is. The Poisson ratio (v) can also be used to describe the ductility or brittleness, and the material will have higher ductility with the increase of v [35]. From the results in Fig. 12, the ductility of $(CoNiCuMo)_{1-x}W_x$ HEAs decreases with increasing W mole fraction.

In order to study the anisotropy of elasticity, we calculated elastic modulus of $(CoNiCuMo)_{1-x}W_x$ HEAs in different crystal orientations, as shown in Fig. 13. With increasing W content, the anisotropy of elastic modulus is more obvious.

In order to explain the influencing mechanism of W content on the elastic properties of $(CoNiCuMo)_{1-x}W_x$ HEAs, we calculated the charge density difference, as shown in Fig. 14. Noticeable

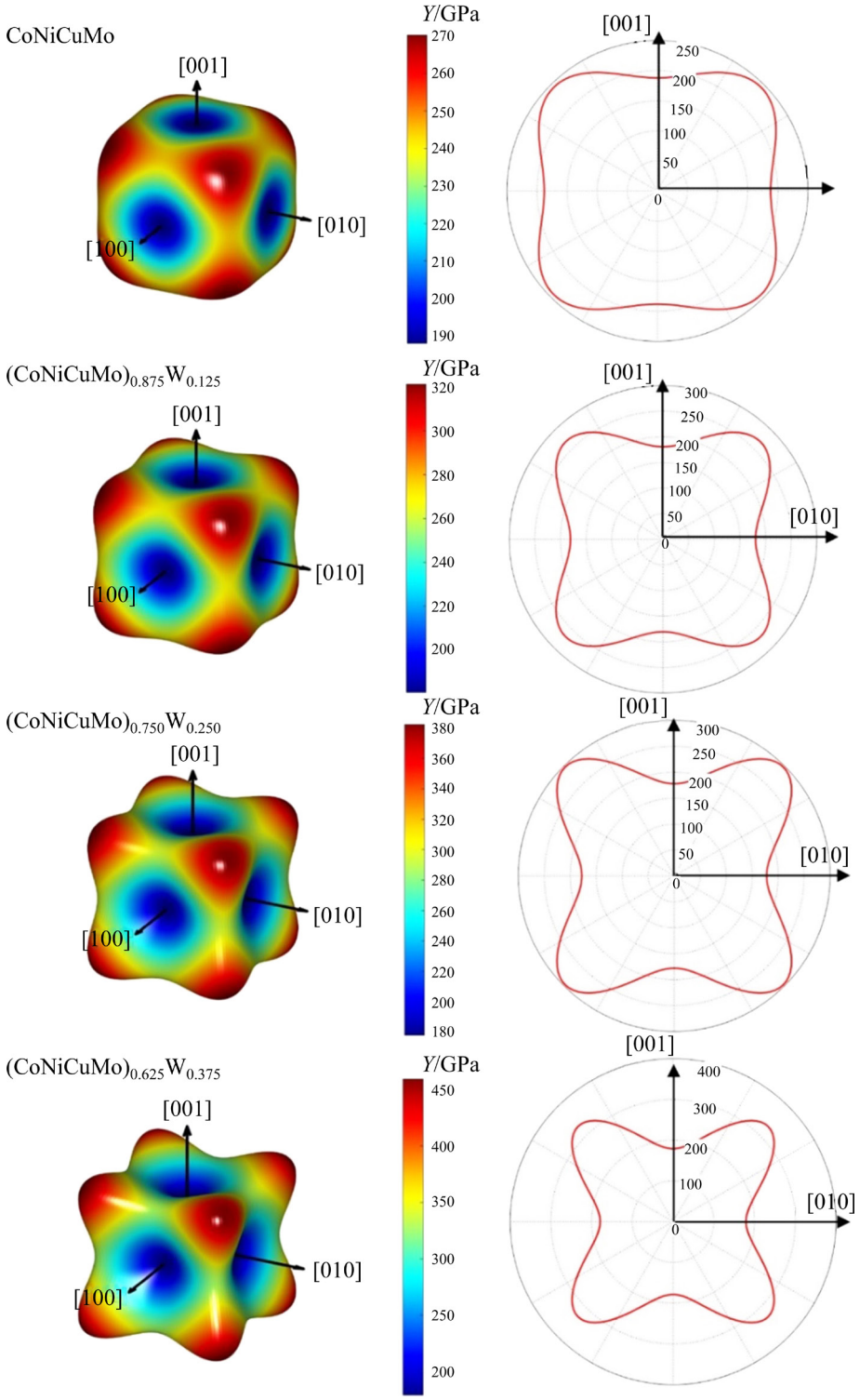

Fig. 13 Elastic modulus of $(CoNiCuMo)_{1-x}W_x$ HEAs in different crystal orientations

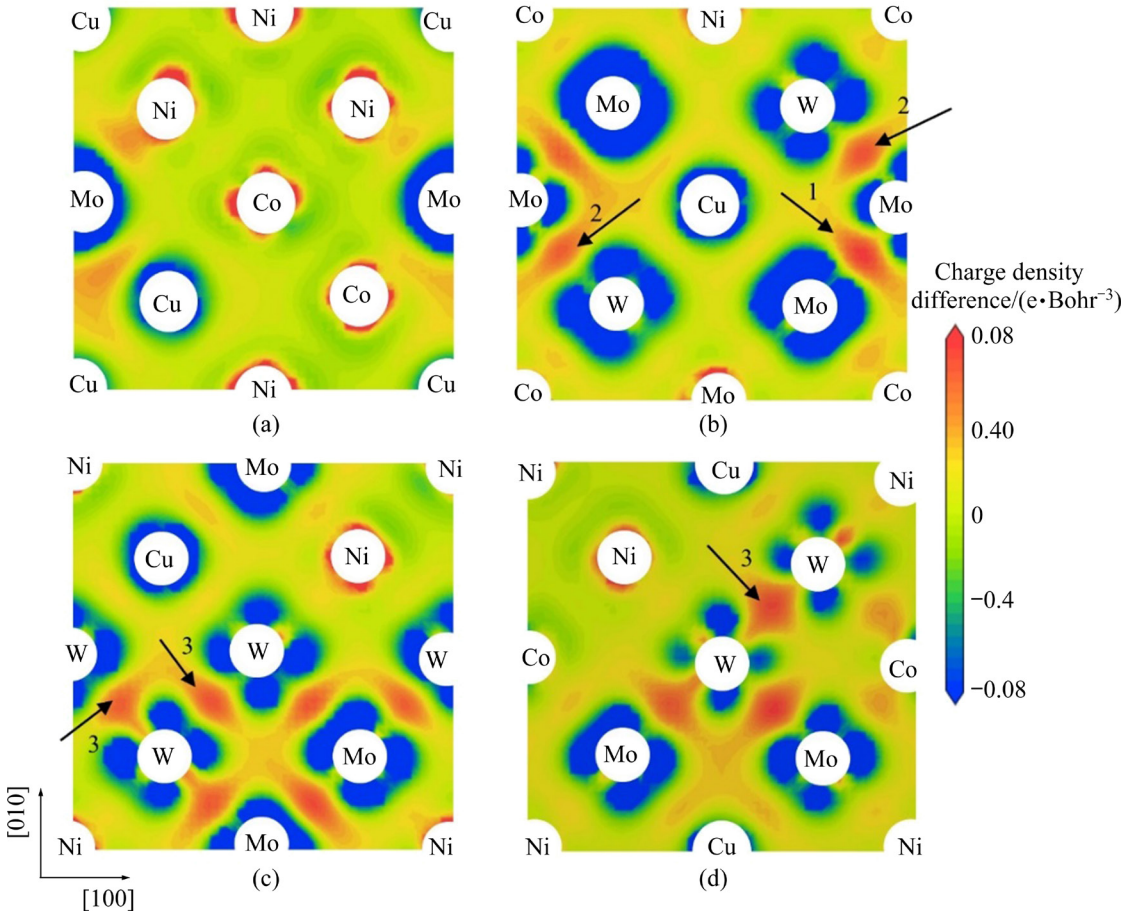

Fig. 14 Charge density difference in $(CoNiCuMo)_{1-x}W_x$ HEAs: (a) CoNiCuMo; (b) $(CoNiCuMo)_{0.875}W_{0.125}$; (c) $(CoNiCuMo)_{0.750}W_{0.250}$; (d) $(CoNiCuMo)_{0.625}W_{0.375}$

charge accumulation can be seen at Mo—Mo, W—W and W—Mo bonds, indicating the obvious covalent bonds formed between these atoms. The directionality of charge distribution around the W atoms is obvious, which is also the characteristic of covalent bond. The covalent bond usually has strong adhesion but poor plasticity, so the calculation results of stiffness, ductility (Fig. 12) and anisotropy (Fig. 13) can also be verified in Fig. 14.

The above calculations are all about the elastic properties at ground state (T=0 K). The study of elastic properties at high temperature is significant for applying HEAs in engineering field, such as reactor structural materials. Therefore, we also predicted elastic properties at different temperatures by fitting EOS.

The relative volume of the FCC $(CoNiCuMo)_{1-x}W_x$ HEAs varying with pressure is shown in Fig. 15. The relative volumes of the four alloys decrease with increasing external pressure, and the decreasing trend is more obvious at higher temperatures. Besides, it can be found that the resistance to compression of FCC $(CoNiCuMo)_{1-x}W_x$ HEAs increases with increasing W content.

The bulk modulus of FCC $(CoNiCuMo)_{1-x}W_x$ HEAs varying with temperature is shown in Fig. 16. It can be seen that the bulk modulus of the four alloys decreases with increasing temperature, indicating different softening tendencies. At the same temperature and pressure, the bulk modulus of $(CoNiCuMo)_{1-x}W_x$ HEAs increases with increasing W content, indicating that W is helpful for softening resistance. In addition, when the temperature rises from 0 to 1200 K under 0 GPa, the bulk modulus of $(CoNiCuMo)_{0.625}W_{0.375}$ HEAs is decreased by 49 GPa. However, the bulk modulus of CoNiCuMo is decreased by 54 GPa, as shown in Fig. 16(a), which further proves the contribution of W to the softening resistance at high temperatures.

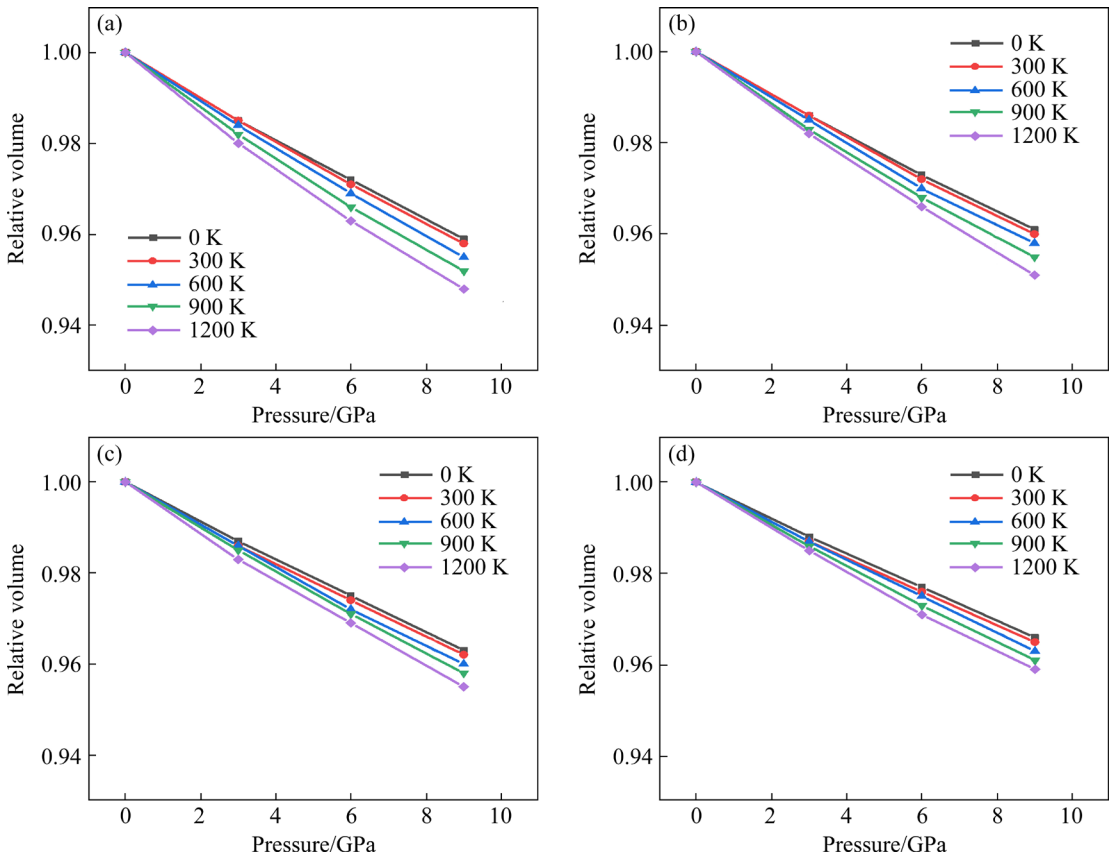

Fig. 15 Relative volume of FCC $(CoNiCuMo)_{1-x}W_x$ HEAs varying with pressure: (a) x=0; (b) x=0.125; (c) x=0.250; (d) x=0.375

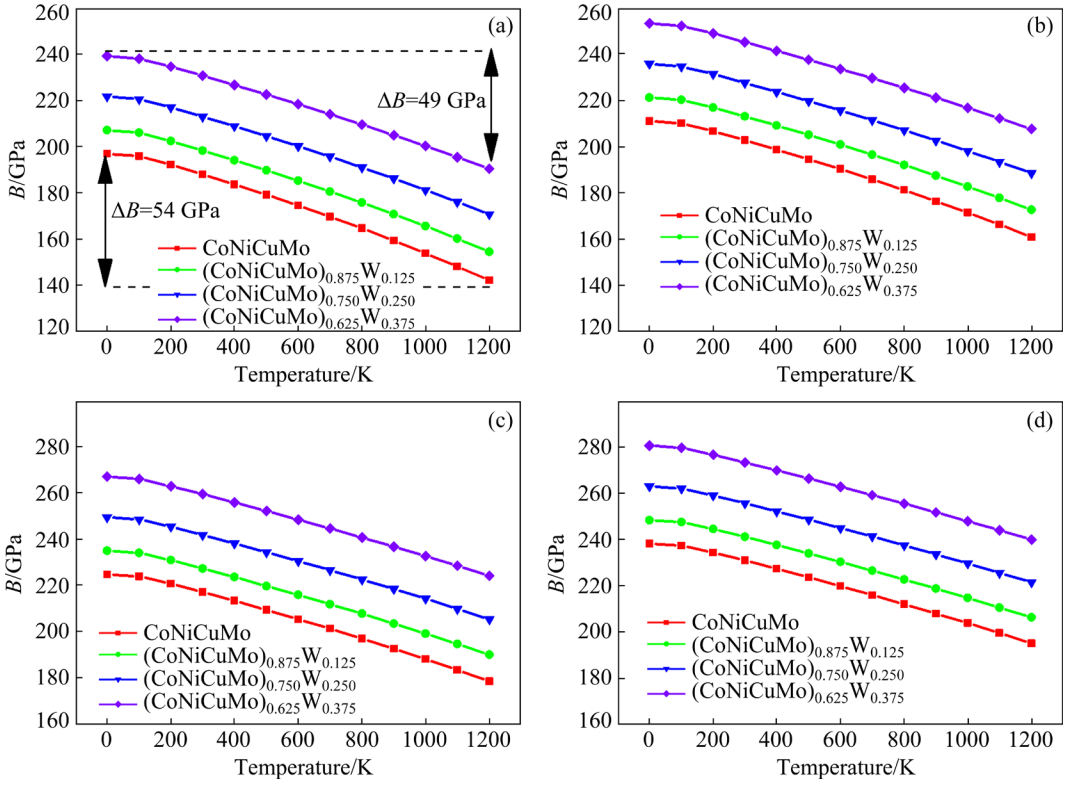

Fig. 16 Bulk modulus (B) of FCC $(CoNiCuMo)_{1-x}W_x$ HEAs varying with temperature at different pressures: (a) 0 GPa; (b) 3 GPa; (c) 6 GPa; (d) 9 GPa

4 Conclusions

(1) GBDT performs well for predicting elastic modulus of FCC HEAs, and the R^2 of predicted B and G in the test set are 0.81 and 0.84, respectively. CoNiCuMoW HEAs have the largest B, G, Y and good ductility (G/B≤0.57) among the FCC HEAs with equal components. Besides, W is a critical element according to the results from ML.

(2) The elastic anisotropy of $(CoNiCuMo)_{1-x}W_x$ HEAs increases while the Cauchy pressure and Poisson ratio decrease with increasing W content from the first-principles calculation. There is obvious charge accumulation at W—W and W—Mo bonds and directional covalent bonds formed between W atoms and their neighboring atoms from the analysis of charge density difference.

(3) The results of elastic properties obtained by fitting EOS show that the resistance to compression and softening of FCC $(CoNiCuMo)_{1-x}W_x$ HEAs at high temperatures increase with the increase of W content.

Acknowledgments

The authors are grateful for the financial support from the National Natural Science Foundation of China (Nos. 62173280, 51975491).

References

[1] GLUDOVATZ B, HOHENWARTER A, CATOOR D, CHANG E H, GEORGE E P, RITCHIE R O. A fracture-resistant high-entropy alloy for cryogenic applications [J]. Science, 2014, 345: 1153−1158.

[2] LU Chen-yang, NIU Liang-liang, CHEN Nan-jun, JIN Ke, YANG Tai-ni, XIU Peng-yuan, ZHANG Yan-wen, GAO fei, BEI Hong-bin, SHI Shi, HE M R, ROBERTSON I M, WEBER W J, WANG Lu-min. Enhancing radiation tolerance by controlling defect mobility and migration pathways in multicomponent single-phase alloys [J]. Nature Communications, 2016, 7: 13564.

[3] GRANBERG F, NORDLUND K, ULLAH M W, JIN K, LU C, BEI H, WANG L M, DJURABEKOVA F, WEBER W J, ZHANG Y. Mechanism of radiation damage reduction in equiatomic multicomponent single phase alloys [J]. Physical Review Letters, 2016, 116: 135504.

[4] NAGASE T, RACK P D, NOH J H, EGAMI T. In-situ TEM observation of structural changes in nano-crystalline CoCrCuFeNi multicomponent high-entropy alloy (HEA) under fast electron irradiation by high voltage electron microscopy (HVEM) [J]. Intermetallics, 2015, 59: 32−42.

[5] ZHANG Yan-wen, STOCKS G M, JIN Ke, LU Chen-yang, BEI Hong-bin, SALES B C, WANG Lu-min, BÉLAND L K, STOLLER R E, SAMOLYUK G D, CARO M, CARO A, WEBER W J. Influence of chemical disorder on energy dissipation and defect evolution in concentrated solid solution alloys [J]. Nature Communications, 2015, 6: 8736.

[6] TUNES M A, LE H, GREAVES G, SCHÖN C G, BEI Hong-bin, ZHANG Yan-wen, EDMONDSON P D, DONNELLY S E. Investigating sluggish diffusion in a concentrated solid solution alloy using ion irradiation with in situ TEM [J]. Intermetallics, 2019, 110: 106461.

[7] XIA S Q, YANG X, YANG T F, LIU S, ZHANG Y. Irradiation resistance in $Al_xCoCrFeNi$ high entropy alloys [J]. JOM, 2015, 67: 2340−2344.

[8] MAKUCH N. Influence of nickel silicides presence on hardness, elastic modulus and fracture toughness of gas-borided layer produced on Nisil-alloy [J]. Transactions of Nonferrous Metals Society of China, 2021, 31: 764−778.

[9] ZENG Wei-jing, HU Kun, LIU Hua-shan, PENG Hai-long, CAI Ge-mei, JIN Zhan-peng. Crystal structures and elastic properties of $Ti(Cu,Pt)_2$ and $Ti(Cu,Pt)_3$ phases [J]. Transactions of Nonferrous Metals Society of China, 2020, 30: 1839−1848.

[10] DAI Xiang, JIANG Fu-lin, LIU Jin, WU Luo-yi, FU Ding-fa, TENG Jie, ZHANG Hui. Strain anisotropy models for refined diffraction line profile analysis in cubic metals [J]. Transactions of Nonferrous Metals Society of China, 2020, 30: 2090−2106.

[11] ZHANG Hua-lei, SUN Xun, LU Song, DONG Zhi-hua, DING Xiang-dong, WANG Yun-zhi, VITOS L. Elastic properties of $Al_xCrMnFeCoNi$ ($0≤x≤5$) high-entropy alloys from ab initio theory [J]. Acta Materialia, 2018, 155: 12−22.

[12] ZHAO Qing-kun, LI Jia, FANG Qi-hong, FENG Hui. Effect of Al solute concentration on mechanical properties of $Al_xFeCuCrNi$ high-entropy alloys: A first-principles study [J]. Physica B: Condensed Matter, 2019, 566: 30−37.

[13] AYDIN F, DURGUT R. Estimation of wear performance of AZ91 alloy under dry sliding conditions using machine learning methods [J]. Transactions of Nonferrous Metals Society of China, 2021, 31: 125−137.

[14] SHI Ze-yan, QUAN Guo-zheng, AN Chao, QIU Hui-min, WANG Wei-yong, ZHANG Zhi-hua. Artificial intelligence model of complicated flow behaviors for Ti−13Nb−13Zr alloy and relevant applications [J]. Transactions of Nonferrous Metals Society of China, 2019, 29: 2090−2098.

[15] ZHOU Zi-qing, ZHOU Ye-ju, HE Quan-feng, DING Zhao-yi, LI Fu-cheng, YANG Yong. Machine learning guided appraisal and exploration of phase design for high entropy alloys [J]. NPJ Computational Materials, 2019, 5: 128.

[16] ROY A, BABUSKA T, KRICK B, BALASUBRAMANIAN G. Machine learned feature identification for predicting phase and Young's modulus of low-, medium- and high-entropy alloys [J]. Scripta Materialia, 2020, 185: 152−158.

[17] SEGALL M D, LINDAN P J D, PROBERT M J, PICKARD C J, HASNIP P J, CLARK S J, PAYNE M C. First-principles simulation: Ideas, illustrations and the CASTEP code [J]. Journal of Physics: Condensed Matter, 2002, 14: 2717−2744.

[18] MONKHORST H J, PACK J D. Special points for Brillouin-zone integrations [J]. Physical Review B, 1976, 13: 5188−5192.
[19] ZUNGER A, WEI S H, FERREIRA L G, BERNARD J E. Special quasirandom structures [J]. Physical Review Letters, 1990, 65: 353−356.
[20] van de WALLE A, TIWARY P, de JONG M, OLMSTED D L, ASTA M, DICK A, SHIN D, WANG Y, CHEN L Q, LIU Z K. Efficient stochastic generation of special quasirandom structures [J]. Calphad-computer Coupling of Phase Diagrams and Thermochemistry, 2013, 42: 13−18.
[21] TASNÁDI F, ODÉN M, ABRIKOSOV I A. Ab initio elastic tensor of cubic $Ti_{0.5}Al_{0.5}N$ alloys: Dependence of elastic constants on size and shape of the supercell model and their convergence [J]. Physical Review B, 2012, 85: 144112.
[22] von PEZOLD J, DICK A, FRIAK M, NEUGEBAUER J. Generation and performance of special quasirandom structures for studying the elastic properties of random alloys: Application to Al−Ti [J]. Physical Review B, 2010, 81: 94203.
[23] HILL R. The elastic behaviour of a crystalline aggregate [J]. Proceedings of the Physical Society, 1952, 65: 349−354.
[24] OTERO-DE-LA-ROZA A, LUAÑA V. GIBBS2: A new version of the quasi-harmonic model code. I: Robust treatment of the static data [J]. Computer Physics Communications, 2011, 182: 1708−1720.
[25] OTERO-DE-LA-ROZA A, ABBASI-PÉREZ D, LUAÑA V. GIBBS2: A new version of the quasiharmonic model code. II: Models for solid-state thermodynamics, features and implementation [J]. Computer Physics Communications, 2011, 182: 2232−2248.
[26] YANG Xiao, ZHANG Yong. Prediction of high-entropy stabilized solid-solution in multi-component alloys [J]. Materials Chemistry and Physics, 2012, 132: 233−238.
[27] GUO Sheng, NG Chun, LU Jian. Effect of valence electron concentration on stability of fcc or bcc phase in high entropy alloys [J]. Journal of Applied Physics, 2011, 109: 103505.
[28] GAO M C, YEH J W, LIAW P K, ZHANG Y. High-entropy alloys: Fundamentals and applications [M]. Berlin: Springer, 2016.
[29] TIAN Fu-yang, VARGA L K, SHEN Jiang, VITOS L. Calculating elastic constants in high-entropy alloys using the coherent potential approximation: Current issues and errors [J]. Computational Materials Science, 2016, 111: 350−358.
[30] ZADDACH A J, NIU C, KOCH C C, IRVING D L. Mechanical properties and stacking fault energies of NiFeCrCoMn high-entropy alloy [J]. JOM, 2013, 65: 1780−1789.
[31] TANAKA K, TERAMOTO T, ITO R. Monocrystalline elastic constants of fcc-CrMnFeCoNi high entropy alloy [J]. MRS Advances, 2017, 2: 1429−1434.
[32] WU Y, LIU W H, WANG X L, MA D, STOICA A D, NIEH T G, HE Z B, LU Z P. In-situ neutron diffraction study of deformation behavior of a multi-component high-entropy alloy [J]. Applied Physics Letters, 2014, 104: 519105.
[33] HAGLUND A, KOEHLER M, CATOOR D, GEORGE E P, KEPPENS V. Polycrystalline elastic moduli of a high-entropy alloy at cryogenic temperatures [J]. Intermetallics, 2015, 58: 62−64.
[34] PUGH S F. Relations between the elastic moduli and the plastic properties of polycrystalline pure metals [J]. Philosophical Magazine, 1954, 45: 823−843.
[35] MA L S, DUAN Y H, LI R U. Structural, elastic and electronic properties of C14-type Al_2M (M=Mg, Ca, Sr and Ba) Laves phases [J]. Physica B: Condensed Matter, 2017, 507: 147−155.

基于机器学习的面心立方高熵合金弹性性能预测

王 申，李 达，熊 俊

西南交通大学 材料科学与工程学院 材料先进技术教育部重点实验室，成都 610031

摘 要：提出预测面心立方高熵合金弹性性能的机器学习模型。数据集来源于第一性原理计算得到的 186 组样本。测试集体积模量(B)和剪切模量(G)预测值的拟合优度(R^2)分别达到 0.81 和 0.84。根据机器学习结果，CoNiCuMoW 在等主元高熵合金(G/B≤0.57)中具有最高的 B、G 和弹性模量(Y)和良好的塑性。第一性原理计算结果表明，当 W 含量增加时，$(CoNiCuMo)_{1-x}W_x$ 合金的弹性各向异性提高，且塑性下降。差分电荷密度分析结果表明，W—W 和 W—Mo 键存在明显的电荷聚集，表明 W 原子与邻近原子间存在共价键作用。

关键词：弹性模量；面心立方高熵合金；第一性原理计算；机器学习

(Edited by Wei-ping CHEN)